*Journal of Sound and Vibration* (1998) **216**(1), 1–28
*Article No*. sv981644

# COMPLEX EIGENSOLUTIONS OF RECTANGULAR PLATES WITH DAMPING PATCHES

S.-W. KUNG AND R. SINGH

*Acoustics and Dynamics Laboratory, Department of Mechanical Engineering, The Ohio State University, Columbus, OH* 43210-1107, *U.S.A.*

(*Received* 20 *August* 1997, *and in final form* 9 *March* 1998)

A new analytical, energy based approach that predicts the vibration characteristics of a rectangular plate with multiple viscoelastic patches is presented. This paper extends the method presented earlier by the authors that was applied to the determination of the eigensolutions of viscoelastically damped beams. The method first relates all motion variables of a sandwich plate in terms of the flexural displacement of the base structure. Then the flexural shape function sets are incorporated in the Rayleigh–Ritz minimization scheme to obtain a complex eigenvalue problem. This method allows for the visualization of complex modes of all deformation variables including shear deformations of the viscoelastic core that are the major contributors to the overall energy dissipation. Comparison with the work of three prior investigators on a simply supported plate validates the model for the limiting case of full coverage. Benchmark experimental measurements are made on a plate with free edges, and five damping cases are considered. Analytical predictions of natural frequencies, modal loss factors and complex modes for all cases are in excellent agreement with modal measurements. A normalization scheme for complex mode shapes has also been developed. Finally, simplified loss factor estimation procedures are presented to illustrate the additive effect of two damping patches.



## 1. INTRODUCTION

In many practical plate and machinery casing structures, it is difficult to treat the whole surface with constrained layer viscoelastic material. Further, it may indeed be desirable to selectively apply one or more damping patches to control certain resonances. To study such issues, an efficient analytical method is needed to predict modal properties of a damped structure. Therefore, the research problem is formulated in the context of a rectangular plate with arbitrary boundary conditions. Complex eigensolutions are sought for various damping cases including full and partial coverage, as well as the configuration with multiple damping patches. The method proposed in this paper first relates motion variables for all layers of a sandwich plate in terms of the flexural displacement of the base plate by using well-known equations of sandwich structures [1–5] and a minimization scheme. Then the flexural shape function sets constructed by $N_x$ and $N_y$ shape functions in $x$ and $y$ directions are incorporated in the Rayleigh–Ritz minimization scheme to obtain a complex eigenvalue problem of dimension $N_x \times N_y$. This formulation yields efficient calculations of various modal deformations in all layers. This work is an extension of the analytical and experimental methodology we proposed recently for sandwich beams [1].

There is a vast body of literature on the dynamic analysis of sandwich beams and plates as evident from the extensive references cited in two books on vibration damping [2, 3]. Most of the publications consider only the full damping coverage, however, Lall *et al*. [4] have addressed the partial coverage issue. They analyzed a simply supported plate with

0022–460X/98/360001 + 28 $30.00/0 

a single damping patch using the Rayleigh–Ritz method and calculated the natural frequencies and modal loss factors. A parametric study on the patch size and location was reported. No experimental results were provided but the full coverage case was compared with an analysis carried out earlier by Mead, as reported in reference [4]. This simply supported plate case will be studied again in this article for the sake of verification. Limiting case results of He and Ma [5] will also be included and compared with other predictions. Since no prior experimental results are available, benchmark modal measurements are conducted on a plate with free edges for several damping configurations. Our method is then validated by comparing complex eigensolution predictions with modal measurements. A normalization scheme for viewing complex modes is also developed. Finally, design-oriented loss factor estimation procedures that examine the additive effect of two damping patches are proposed.

## 2. ANALYTICAL FORMULATION

### 2.1. PHYSICAL EXAMPLE

The structure of interest is a rectangular plate with $N_p$ damping patches attached, as shown in Figure 1. Each patch $p$ is of length $l_x^p$ and width $l_y^p$ and is located at $(x^p, y^p)$ in the Cartesian co-ordinates. Each patch has two layers: layer 1 is a metallic layer while layer 2 is made of the viscoelastic material. Note that each patch may be different in size, thickness and material property. The base plate is assumed to be undamped and is designated as layer 3. The boundary conditions are specified later when eigensolutions are sought. Figure 2 shows sections of the plate in the $xz$ and $yz$ planes. All relevant variables considered include: flexural $w(x, y; t)$ displacement in the $z$ direction, and in-plane displacements $u(x, y; t)$ and $v(x, y; t)$ along $x$ and $y$, respectively, and rotary ($\psi$) and shear angles ($\gamma$) in the $xz$ and $yz$ planes. These variables are included in three deformation vectors $\mathbf{r}_1^p$, $\mathbf{r}_2^p$, and $\mathbf{r}_3$,

$$\mathbf{r}_1^p = \begin{bmatrix} w \\ u_1^p \\ v_1^p \\ \psi_{xz,1}^p \\ \psi_{yz,1}^p \end{bmatrix}, \quad \mathbf{r}_2^p = \begin{bmatrix} w \\ u_2^p \\ v_2^p \\ \psi_{xz,2}^p \\ \psi_{yz,2}^p \end{bmatrix}, \quad \mathbf{r}_3 = \begin{bmatrix} w \\ u_3 \\ v_3 \\ \psi_{xz,3} \\ \psi_{yz,3} \end{bmatrix}; \qquad p = 1, \ldots, N_p, \quad \text{(1a–c)}$$

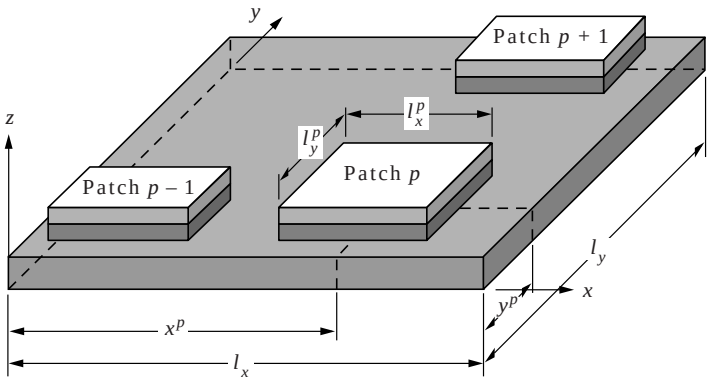


Figure 1. Multiple constrained layer damping patches for a rectangular thin plate with arbitrary boundary conditions.

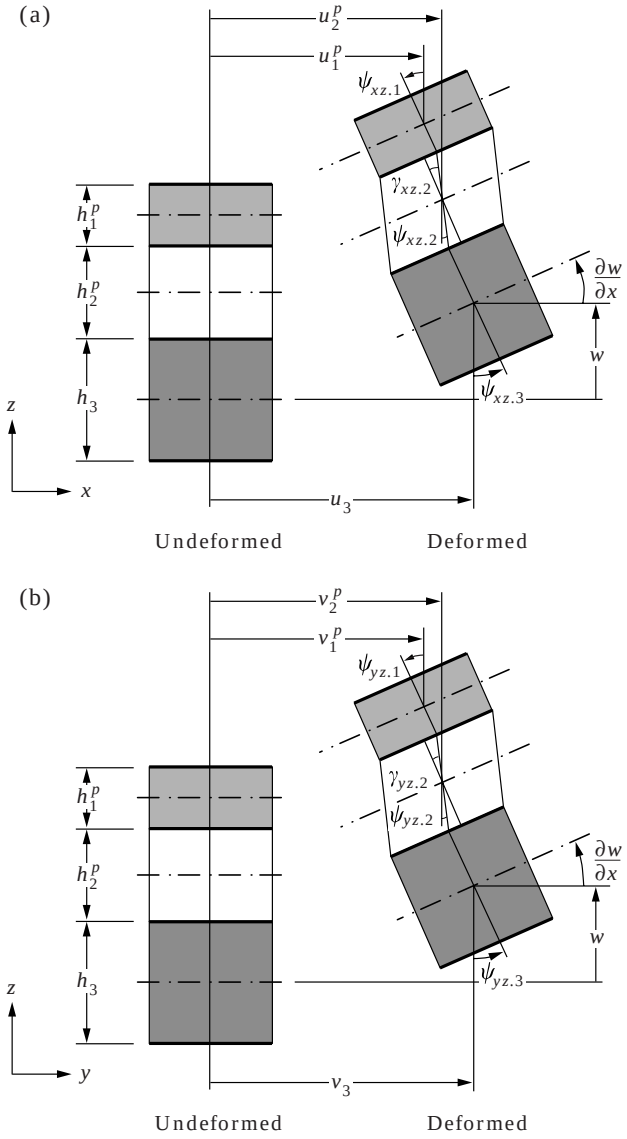


Figure 2. Undeformed and deformed segments along with variables in all layers. (a) $xz$ plane, (b) $yz$ plane.

where subscripts 1, 2 and 3 denote the layer numbers. Note that shear deformations are not included here because they can be obtained from the spatial derivatives of $w(x, y; t)$ and the rotation of layer 2. For elastic layers 1 and 3, shear deformations are assumed to be zero for the sake of simplification.

## 2.2. ENERGY FORMULATION

The strain energy ($U$) of the composite plate with reference to Figures 1 and 2 is written as

$$U = \sum_{p=1}^{N_p} \iint_p [\tfrac{1}{2}(\mathscr{D}\mathbf{r}_1^p)^{\mathrm{T}}\mathbf{E}_1^p(\mathscr{D}\mathbf{r}_1^p) + \tfrac{1}{2}(\mathscr{D}\mathbf{r}_2^p)^{\mathrm{T}}\mathbf{E}_2^p(\mathscr{D}\mathbf{r}_2^p)]\,\mathrm{d}x\,\mathrm{d}y + \int_0^{l_y}\int_0^{l_x} \tfrac{1}{2}(\mathscr{D}\mathbf{r}_3)^{\mathrm{T}}\mathbf{E}_3(\mathscr{D}\mathbf{r}_3)\,\mathrm{d}x\,\mathrm{d}y, \quad (2)$$

TABLE 1

*System parameters used for rectangular plate example as described in the literature* [4]. *All edges assume simple supports. Refer to Figure* 1 *for nomenclature*

| | | Example I [4] | Example II [4] |
|---|---|---|---|
| Material properties | $E_1$ and $E_3$ (Pa) | $207 \times 10^9$ | $207 \times 10^9$ |
| | $G_2$ (Pa) | $4 \times 10^6$ | $450 \times 10^6$ |
| | $\eta_2$ | 0·38 | 0·38 |
| | $\rho_1$ and $\rho_3$ (kg/m$^3$) | 7800 | 7800 |
| | $\rho_2$ (kg/m$^3$) | 2000 | 2000 |
| Dimensions (mm) | $h_1$ | 5 | 2·5 |
| | $h_2$ | 5 | 2·5 |
| | $h_3$ | 5 | 5 |
| | $l_x$ | 400 | 400 |
| | $l_y$ | 400 | 400 |

where $\mathscr{D}$ is the differential operator matrix defined as

$$\mathscr{D} = \begin{bmatrix} \partial^2/\partial x^2 & 0 & 0 & 0 & 0 \\ \partial^2/\partial x\,\partial y & 0 & 0 & 0 & 0 \\ \partial^2/\partial y^2 & 0 & 0 & 0 & 0 \\ 0 & \partial/\partial x & 0 & 0 & 0 \\ 0 & 0 & \partial/\partial y & 0 & 0 \\ 0 & \partial/\partial y & 0 & 0 & 0 \\ 0 & 0 & \partial/\partial x & 0 & 0 \\ \partial/\partial x & 0 & 0 & -1 & 0 \\ 0 & \partial/\partial y & 0 & 0 & -1 \end{bmatrix}, \tag{3}$$

TABLE 2

*Comparison between published* [4, 5] *and proposed methods for Example I. See Table* 1 *for rectangular plate parameters*

| | Lall *et al*. [4] | Mead [4] | He and Ma [5] | Proposed |
|---|---|---|---|---|
| Natural frequency $\omega$ (rad/s) | | | | |
| Mode (1, 1) | 975·17 | 975·00 | 975·00 | 974·91 |
| Mode (1, 2) | 2350·79 | 2350·83 | 2350·80 | 2350·80 |
| Mode (2, 1) | 2350·79 | 2350·83 | 2350·80 | 2350·80 |
| Mode (2, 2) | 3725·33 | 3725·60 | 3725·60 | 3725·60 |
| Loss factor $\eta$ (%) | | | | |
| Mode (1, 1) | 4·431 | 4·385 | 4·385 | 4·386 |
| Mode (1, 2) | 1·918 | 1·911 | 1·911 | 1·911 |
| Mode (2, 1) | 1·918 | 1·911 | 1·911 | 1·911 |
| Mode (2, 2) | 1·224 | 1·221 | 1·221 | 1·221 |

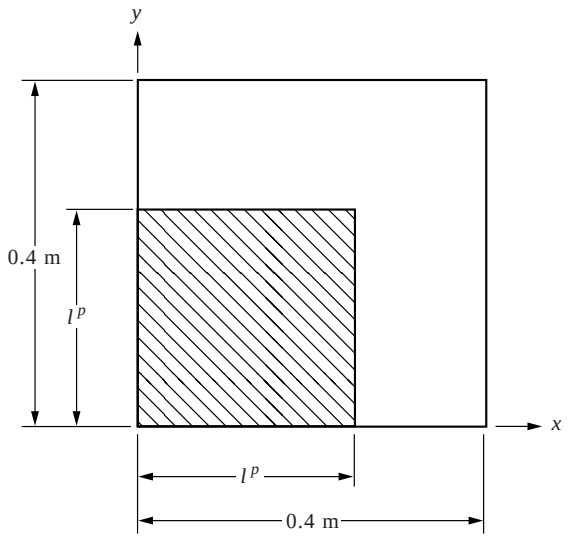


Figure 3. Patch size and location for Example II, as by Lall *et al*. [4]. The base plate is simply supported on all edges. Here $l_p$ varies from 0 to 0·4 m. Refer to Table 1 for more details.

and $\mathbf{E}_1^p$, $\mathbf{E}_2^p$ and $\mathbf{E}_3$ are elasticity matrices that are defined as

$$\mathbf{E}_i^p = \begin{bmatrix} \mathbf{E}_{w,i}^p & \mathbf{0} & \mathbf{0} \\ \mathbf{0} & \mathbf{E}_{uv,i}^p & \mathbf{0} \\ \mathbf{0} & \mathbf{0} & \mathbf{E}_{\gamma,i}^p \end{bmatrix}, \qquad p = 1, \ldots, N_p \text{ for } i = 1, 2; \quad i = 1, 2, 3; \tag{4}$$

where

$$\mathbf{E}_{w,i}^p = \frac{E_i^p (h_i^p)^3}{12(1 - v_i^2)} \begin{bmatrix} 1 & 0 & v_i \\ 0 & 2(1 - v_i) & 0 \\ v_i & 0 & 1 \end{bmatrix}, \tag{5a}$$

$$\mathbf{E}_{uv,i}^p = \frac{E_i^p (h_i^p)^3}{2(1 - v_i^2)} \begin{bmatrix} 1 & v_i & 0 & 0 \\ v_i & 1 & 0 & 0 \\ 0 & 0 & (1 - v_i)/2 & (1 - v_i)/2 \\ 0 & 0 & (1 - v_i)/2 & (1 - v_i)/2 \end{bmatrix},$$

$$\mathbf{E}_{\gamma,i}^p = G_i^p h_i^p \begin{bmatrix} 1 & 0 \\ 0 & 1 \end{bmatrix}, \tag{5b, c}$$

and $E$, $G$, $v$ and $h$ are Young's modulus, shear modulus, Poisson's ratio and thickness, respectively. The kinetic energy ($T$) of the composite plate due to flexural, longitudinal and rotary motions is expressed as

$$T = \sum_{p=1}^{N_p} \int\int_p [\tfrac{1}{2} \dot{\mathbf{r}}_1^{pT} \mathbf{H}_1 \dot{\mathbf{r}}_1^p + \tfrac{1}{2} \dot{\mathbf{r}}_2^{pT} \mathbf{H}_2 \dot{\mathbf{r}}_2^p] \, dx \, dy + \int_0^{l_y} \int_0^{l_x} \frac{1}{2} \dot{\mathbf{r}}_3^T \mathbf{H}_3 \dot{\mathbf{r}}_3 \, dx \, dy, \tag{6}$$

where

$$\mathbf{H}_i^p = \rho_1^p \begin{bmatrix} h_i^p & & & & \mathbf{0} \\ & h_i^p & & & \\ & & h_i^p & & \\ & & & (h_i^p)^3/12 & \\ \mathbf{0} & & & & (h_i^p)^3/12 \end{bmatrix}, \qquad p = 1, \ldots, N_p \quad \text{for} \quad i = 1, 2: \; i = 1, 2, 3 \tag{7}$$

### 2.3. RITZ SHAPE FUNCTIONS

To implement the Rayleigh–Ritz minimization scheme, deformation vectors are approximated as

$$\mathbf{r}_1^p(x, y, t) = \mathbf{S}_1^p(x, y)\mathbf{q}(t), \qquad \mathbf{r}_2^p(x, y, t) = \mathbf{S}_2^p(x, y)\mathbf{q}(t), \qquad \mathbf{r}_3(x, y, t) = \mathbf{S}_3(x, y)\mathbf{q}(t), \tag{8a–c}$$

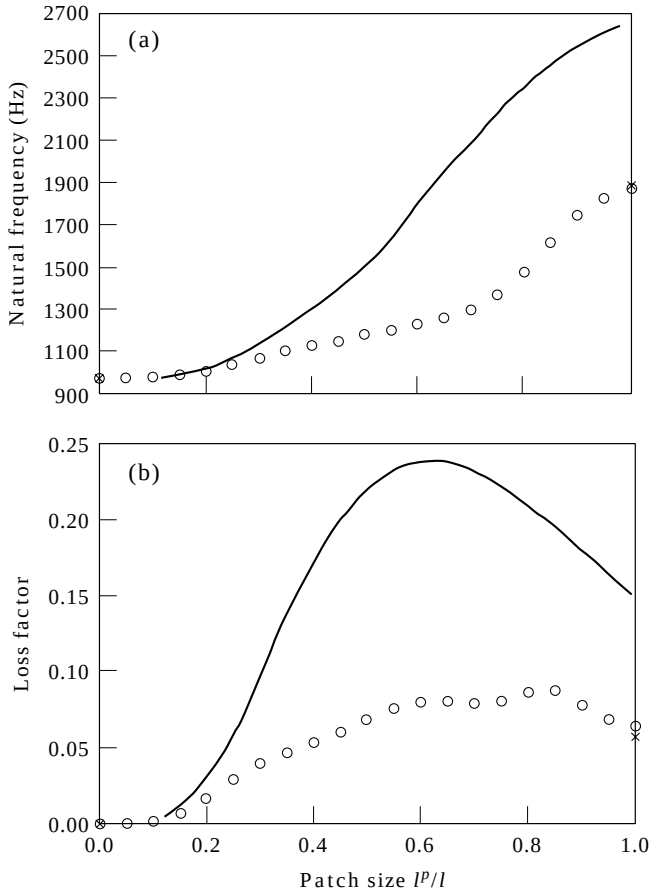


Figure 4. Comparison between published and proposed methods for Example II. (a) First natural frequency; (b) first modal loss factor. ○, Proposed method; ×, He and Ma [5]; —, Lall *et al*. [4].

TABLE 3

*Properties of sandwich plate used for benchmark experiments*

| | | Stiffness ($N/m^2$) | Density ($kg/m^3$) | Thickness (mm) | Material loss factor $\eta_2(f)$ |
|---|---|---|---|---|---|
| Base plate[a] | Layer 3 | $E_3 = 180 \times 10^9$ | $\rho_3 = 7350$ | $h_3 = 2{\cdot}4$ | |
| Patch A[b] | Layer 1 | $E_1 = 180 \times 10^9$ | $\rho_1 = 7720$ | $h_1 = 0{\cdot}79$ | |
| | Layer 2 | $G_2 = 0{\cdot}25 \times 10^6$ | $\rho_2 = 2000$ | $h_2 = 0{\cdot}051$ | $\eta_{2,A}(f) = 4{\cdot}07 \times 10^{-3} f - 0{\cdot}112$ |
| Patch B[b] | Layer 1 | $E_1 = 180 \times 10^9$ | $\rho_1 = 7720$ | $h_1 = 0{\cdot}43$ | |
| | Layer 2 | $G_2 = 0{\cdot}25 \times 10^6$ | $\rho_2 = 2000$ | $h_2 = 0{\cdot}051$ | $\eta_{2,B}(f) = 1{\cdot}06 \times 10^{-3} f + 0{\cdot}131$ |

[a] $342{\cdot}9 \times 266{\cdot}7$ mm with F–F–F–F boundary.

[b] Material provided by the Wolverine Gasket Company. Codes for the patches are: A = WXP-1828, B = WXP-18070.

where $\mathbf{q}$ is the column vector of generalized displacements of the system, and $\mathbf{S}_1^p$, $\mathbf{S}_2^p$ and $\mathbf{S}_3$ are shape function matrices with $N_s$ admissible function sets

$$\mathbf{S}_1^p = [\mathbf{S}_{1,1}^p \quad \cdots \quad \mathbf{S}_{1,k}^p \quad \cdots \quad \mathbf{S}_{1,N_s}^p], \qquad \mathbf{S}_2^p = [\mathbf{S}_{2,1}^p \quad \cdots \quad \mathbf{S}_{2,k}^p \quad \cdots \quad \mathbf{S}_{2,N_s}^p], \quad (9a, b)$$

$$\mathbf{S}_3 = [\mathbf{S}_{3,1} \quad \cdots \quad \mathbf{S}_{3,k} \quad \cdots \quad \mathbf{S}_{3,N_s}]. \quad (9c)$$

Note that $\mathbf{S}_{1,k}^p$, $\mathbf{S}_{2,k}^p$ and $\mathbf{S}_{3,k}$ are the $k$th shape function set of the deformation variables of layers 1, 2 and 3, respectively:

$$\mathbf{S}_{1,k}^p = \begin{bmatrix} \phi_{w,k} \\ \phi_{u1,k}^p \\ \phi_{v1,k}^p \\ \phi_{\psi x1,k}^p \\ \phi_{\psi y1,k}^p \end{bmatrix}, \qquad \mathbf{S}_{2,k}^p = \begin{bmatrix} \phi_{w,k} \\ \phi_{u2,k}^p \\ \phi_{v2,k}^p \\ \phi_{\psi x2,k}^p \\ \phi_{\psi y2,k}^p \end{bmatrix}, \qquad \mathbf{S}_3 = \begin{bmatrix} \phi_{w,k} \\ \phi_{u3,k} \\ \phi_{v3,k} \\ \phi_{\psi x3,k} \\ \phi_{\psi y3,k} \end{bmatrix}; \qquad p = 1, \ldots, N_p. \quad (10)$$

Here the flexural shape function $\phi_{w,k}(x, y)$ is the $k$th element of the flexural shape function row vector $\mathbf{\Phi}_w = [\phi_{w,1} \cdots \phi_{w,k} \cdots \phi_{w,N_s}]$. Note that $\mathbf{\Phi}_w(x, y)$ is obtained from the following equation where $\mathbf{X}_w(x)$ is a column vector of dimension $N_x$ and $\mathbf{Y}_w(x)$ is a row vector of dimension $N_y$. Elements of $\mathbf{X}_w$ and $\mathbf{Y}_w$ must be chosen such that they satisfy the geometrical boundary conditions of the plate in the $x$ and $y$ directions, respectively:

$$\mathbf{\Phi}_w(x, y) = \text{Col}\,[\mathbf{X}_w(x)\mathbf{Y}_w(y)], \quad (11)$$

where Col is a matrix operator that converts a matrix of dimension $(N_x, N_y)$ to a row vector of dimension $N_s = N_x \times N_y$. This operation assigns element $(m, n)$ of the matrix to element $k$ of the row vector where $k = (m-1)N_y + n$; $m = 1 \cdots N_x$, and $n = 1 \cdots N_y$. The flexural shape function $\phi_{w,k}(x, y)$ is used as the "master" shape function vector while all other shape functions are "slaves" and should be calculated from $\phi_{w,k}(x, y)$. Some of the slave shape functions can be obtained explicitly while the rest must be solved for by a minimization scheme.

## 3. SHAPE FUNCTION REDUCTION

Some of the shape functions, as defined earlier by equation (10), can be deduced directly from their kinematic relationships with $\phi_{w,k}$. First, relationships between in-plane shape functions of layers 1 and 3 are employed which can be written by extending the integrated form of the weak core assumption as stated in reference [1]:

$$\phi^p_{u1,k} = -e^p \phi_{u3,k} + d^p_{x,k}, \qquad \phi^p_{v1,k} = -e^p \phi_{v3,k} + d^p_{y,k}, \tag{12a, b}$$

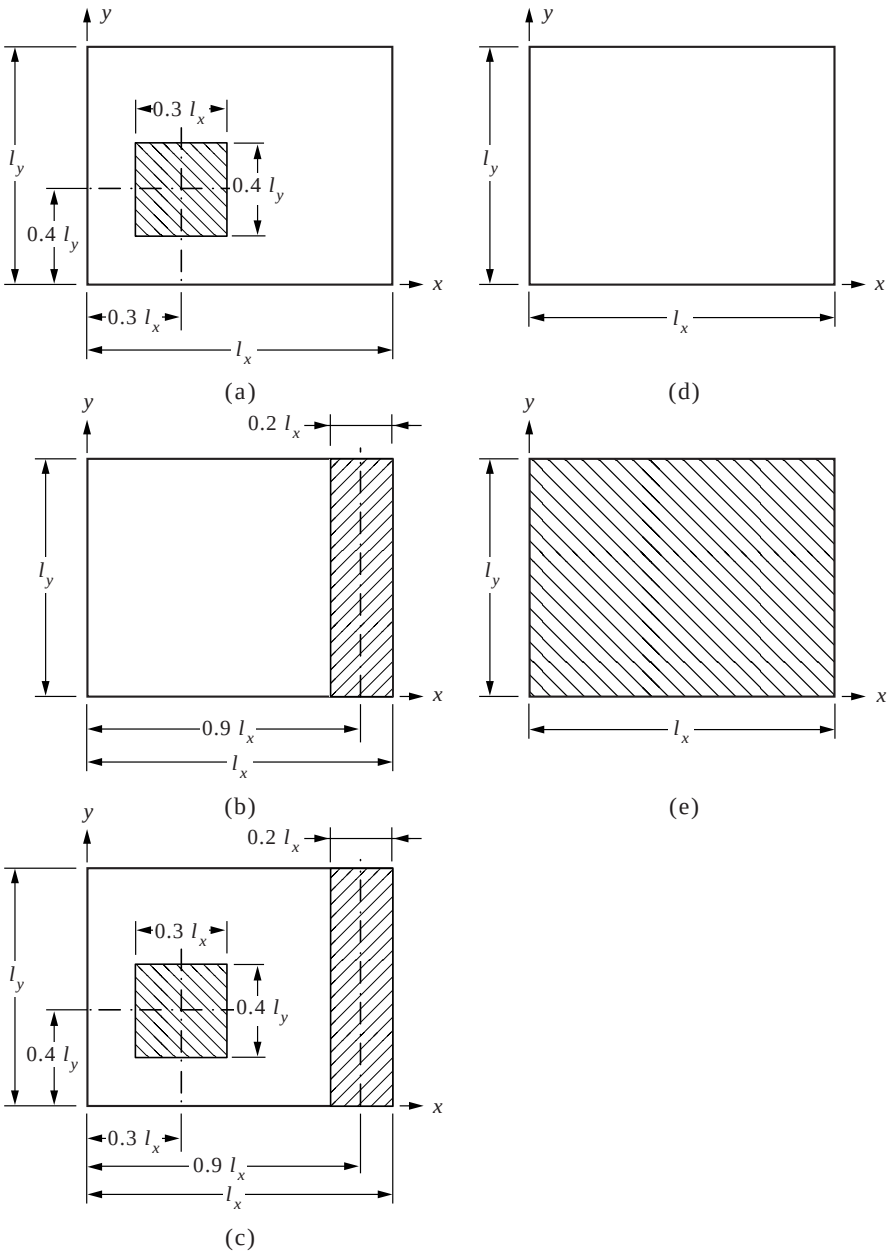


Figure 5. Damping patch cases for the benchmark plate used for experiments studies. (a) Case A; (b) Case B; (c) Case C; (d) Case D; (e) Case E. All edges are free.

TABLE 4

*Modal indices for the benchmark plate example*

| Mode $r$ | Natural frequency range (Hz) from theory | Modal index[a] |
|---|---|---|
| 1 | 83 ~ 94 | (2, 2) |
| 2 | 109 ~ 124 | (2, 0) |
| 3 | 184 ~ 190 | (0, 2) |
| 4 | 199 ~ 207 | (2, 1) |
| 5 | 243 ~ 255 | (1, 2) |
| 6 | 291 ~ 308 | (3, 0) |
| 7 | 377 ~ 406 | (3, 1) |
| 8 | 385 ~ 411 | (2, 2) |

[a] Nodal lines along $x$ and $y$.

where

$$e^p = \frac{E_3 h_3}{E_1^p h_1^p} \frac{[1 - (v_1^p)^2]}{[1 - (v_3^p)^2]}, \qquad p = 1, \ldots, N_p.$$

Note that $d_{x,k}^p$ and $d_{y,k}^p$ are constants that relate deformation shapes $\phi_{u3,k}$ and $\phi_{v3,k}$ to the corresponding $\phi_{u1,k}^p$ and $\phi_{v1,k}^p$ for each patch $p$. Second, the deformations in layer 2 can be rewritten as follows by observing the kinematic relationship in Figure 2:

$$\phi_{u2}^p = \frac{h_1^p - h_3}{4} \frac{\partial \phi_w}{\partial x} + \frac{1 - e^p}{2} \phi_{u3} + \tfrac{1}{2} d_x^p, \qquad \phi_{v2}^p = \frac{h_1^p - h_3}{4} \frac{\partial \phi_w}{\partial y} + \frac{1 - e^p}{2} \phi_{v3} + \tfrac{1}{2} d_y^p, \quad \text{(13a, b)}$$

$$\phi_{\psi x2}^p = -\frac{h_1^p + h_3}{2h_2^p} \frac{\partial \phi_w}{\partial x} + \frac{1 + e^p}{h_2^p} \phi_{u3} - \frac{1}{h_2^p} d_x^p, \qquad \phi_{\psi y2}^p = -\frac{h_1^p + h_3}{2h_2^p} \frac{\partial \phi_w}{\partial y} + \frac{1 + e^p}{h_2^p} \phi_{v3} - \frac{1}{h_2^p} d_y^p. \quad \text{(13c, d)}$$

The $k$th component of the strain energy of plate ($U_k$) with admissible function set $\mathbf{S}_{1,k}^p$, $\mathbf{S}_{2,k}^p$ and $\mathbf{S}_{3,k}$ is as follows where $q_k$ is the corresponding generalized displacement:

$$U_k = \tfrac{1}{2} K_k q_k^2, \tag{14}$$

$$K_k = \sum_{p=1}^{N_p} \iint_p [(\mathscr{D}\mathbf{S}_{1,k}^p)^{\mathrm{T}} \mathbf{E}_1 (\mathscr{D}\mathbf{S}_{1,k}^p) + (\mathscr{D}\mathbf{S}_{2,k}^p)^{\mathrm{T}} \mathbf{E}_2^p (\mathscr{D}\mathbf{S}_{2,k}^p)] \, \mathrm{d}x \, \mathrm{d}y + \int_0^{l_y} \int_0^{l_x} (\mathscr{D}\mathbf{S}_{3,k})^{\mathrm{T}} \mathbf{E}_3 (\mathscr{D}\mathbf{S}_{3,k}) \, \mathrm{d}x \, \mathrm{d}y. \tag{15}$$

Assume that the corresponding displacements $\phi_{u3,k}$ and $\phi_{v3,k}$ are combinations of row trial function vectors $\mathbf{\Psi}_u(x, y)$ and $\mathbf{\Psi}_v(x, y)$:

$$\phi_{u3,k} = \mathbf{\Psi}_u(x, y)\mathbf{c}_{u,k}, \qquad \phi_{v3,k} = \mathbf{\Psi}_v(x, y)\mathbf{c}_{v,k}, \tag{16a, b}$$

where $\mathbf{c}_{u,k}$ and $\mathbf{c}_{v,k}$ are column vectors containing coefficients that need to be determined while $\mathbf{\Psi}_u(x, y)$ and $\mathbf{\Psi}_v(x, y)$ are the row trial function vectors. Both $\mathbf{\Psi}_u(x, y)$ and $\mathbf{\Psi}_v(x, y)$ are obtained from their $x$ components $\mathbf{X}_u(x)$ and $\mathbf{X}_v(x)$ and $y$ components $\mathbf{Y}_u(y)$ and $\mathbf{Y}_v(y)$, respectively:

$$\mathbf{\Psi}_u(x, y) = \mathrm{Col}\,[\mathbf{X}_u(x)\mathbf{Y}_u(y)], \qquad \mathbf{\Psi}_v(x, y) = \mathrm{Col}\,[\mathbf{X}_v(x)\mathbf{Y}_v(y)], \tag{17a, b}$$

where $\mathbf{X}_u$ and $\mathbf{X}_v$ are column vectors of dimension $N_{ux}$ and $N_{vx}$ and $\mathbf{Y}_u$ and $\mathbf{Y}_v$ are row vectors of dimension $N_{uy}$ and $N_{uy}$ whose elements satisfy geometrical boundary conditions in $x$ and $y$ directions, respectively.

By substituting equations (12), (13) and (16) into equation (15) and minimizing $U_k$ with respect to the coefficients of $\mathbf{c}_{u,k}$, $\mathbf{c}_{v,k}$, $d^p_{x,k}$ and $d^p_{y,k}$, a set of governing equations can be formed in matrix form as

$$\mathbf{A}\mathbf{C}_k = \mathbf{B}_k, \tag{18}$$

where

$$\mathbf{A} = \begin{bmatrix} \mathbf{A}^{uu} & \mathbf{A}^{uv} & \mathbf{A}^{u} & \mathbf{0} \\ \mathbf{A}^{vu} & \mathbf{A}^{vv} & \mathbf{0} & \mathbf{A}^{v} \\ (\mathbf{A}^{u})^{\mathrm{T}} & \mathbf{0} & \mathbf{A}^{\mathrm{d}x} & \mathbf{0} \\ \mathbf{0} & (\mathbf{A}^{v})^{\mathrm{T}} & \mathbf{0} & \mathbf{A}^{\mathrm{d}y} \end{bmatrix}, \quad \mathbf{B}_k = \begin{bmatrix} \mathbf{B}^{u}_k \\ \mathbf{B}^{v}_k \\ \mathbf{B}^{\mathrm{d}x}_k \\ \mathbf{B}^{\mathrm{d}y}_k \end{bmatrix}, \quad \mathbf{C}_k = \begin{bmatrix} \mathbf{c}_{u,k} \\ \mathbf{c}_{v,k} \\ \mathbf{d}_{x,k} \\ \mathbf{d}_{y,k} \end{bmatrix}, \tag{19a–c}$$

TABLE 5

*Measured and predicted modal results for the benchmark plate with damping patches as shown in Figure 5*

| Mode | Natural frequency $f_r$ (Hz) | | Modal loss factor $\eta_r$ (%) | |
|---|---|---|---|---|
| | Experiment | Theory | Experiment | Theory |
| Case A (with single Patch A) | | | | |
| (1, 1) | 90 | 84 | 0·32 | 0·22 |
| (2, 0) | 109 | 111 | 0·38 | 0·18 |
| (0, 2) | 199 | 184 | 0·51 | 0·67 |
| (0, 1) | 220 | 207 | 0·43 | 0·44 |
| (1, 2) | 259 | 253 | 0·34 | 0·41 |
| (3, 0) | 329 | 305 | 1·68 | 1·05 |
| (3, 1) | 422 | 405 | 0·39 | 0·32 |
| (0, 2) | 445 | 414 | 0·40 | 0·52 |
| Case B (with single Patch B) | | | | |
| (1, 1) | 86 | 82 | 0·32 | 0·25 |
| (2, 0) | 106 | 109 | 0·24 | 0·01 |
| (0, 2) | 204 | 188 | 1·34 | 1·05 |
| (2, 1) | 214 | 206 | 0·58 | 0·54 |
| (1, 2) | 259 | 255 | 1·52 | 1·36 |
| (3, 0) | 328 | 304 | 0·50 | 0·09 |
| (3, 1) | 416 | 405 | 0·58 | 0·66 |
| (2, 2) | 447 | 414 | 1·20 | 0·92 |
| Case C (with Patches A and B) | | | | |
| (1, 1) | 86 | 82 | 0·52 | 0·52 |
| (2, 0) | 106 | 109 | 0·52 | 0·19 |
| (0, 2) | 200 | 186 | 1·97 | 1·81 |
| (2, 1) | 214 | 207 | 0·88 | 0·93 |
| (1, 2) | 259 | 254 | 1·93 | 1·81 |
| (3, 0) | 322 | 301 | 2·30 | 1·13 |
| (3, 1) | 415 | 404 | 1·00 | 1·07 |
| (2, 2) | 442 | 411 | 1·97 | 1·41 |

TABLE 6

*Measured and predicted modal results for limiting cases of benchmark plate as shown in Figure 5*

| | Natural frequency $f_r$ (Hz) | | Modal loss factor $\eta_r$ (%) | |
|---|---|---|---|---|
| Mode | Experiment | Theory | Experiment | Theory |
| Case D—baseline case (base plate without any patch) | | | | |
| (1, 1) | 89 | 83 | 0·32 | 0 |
| (2, 0) | 107 | 112 | 0·15 | 0 |
| (0, 2) | 202 | 185 | 0·07 | 0 |
| (2, 1) | 218 | 207 | 0·13 | 0 |
| (1, 2) | 257 | 254 | 0·07 | 0 |
| (3, 0) | 336 | 308 | 0·07 | 0 |
| (3, 1) | 420 | 406 | 0·06 | 0 |
| (2, 2) | 447 | 417 | 0·04 | 0 |
| Case E—fully covered case (plate with Patch A material) | | | | |
| (1, 1) | 89 | 94 | 13 | 10 |
| (2, 0) | 111 | 124 | 17 | 12 |
| (0, 2) | 196 | 190 | 13 | 18 |
| (2, 1) | 200 | 199 | 10 | 10 |
| (1, 2) | –[a] | 243 | –[a] | 11 |
| (3, 0) | 314 | 291 | 11 | 15 |
| (3, 1) | 393 | 377 | 10 | 14 |
| (2, 2) | 423 | 385 | 17 | 13 |

[a] Not found in the experiment.

and

$$\mathbf{d}_{x,k} = [d^1_{x,k} \quad \cdots \quad d^p_{x,k} \quad \cdots \quad d^{N_p}_{x,k}]^{\mathrm{T}}, \qquad \mathbf{d}_{y,k} = [d^1_{y,k} \quad \cdots \quad d^p_{y,k} \quad \cdots \quad d^{N_p}_{y,k}]^{\mathrm{T}}. \quad (20a, b)$$

Sub-matrices of $\mathbf{A}$ and sub-vectors of $\mathbf{B}_k$ are obtained from the following:

$$\mathbf{A}^{uu} = \sum_{p=1}^{N_p} \frac{E_3 h_3 e^p}{1-(\nu_3)^2} \iint_p \left[ \left(\frac{\partial}{\partial x}\boldsymbol{\Psi}_u\right)^{\mathrm{T}} \left(\frac{\partial}{\partial x}\boldsymbol{\Psi}_u\right) + \frac{1-\nu_1^p}{2} \left(\frac{\partial}{\partial y}\boldsymbol{\Psi}_u\right)^{\mathrm{T}} \left(\frac{\partial}{\partial y}\boldsymbol{\Psi}_u\right) \right] \mathrm{d}x\, \mathrm{d}y$$

$$+ \sum_{p=1}^{N_p} \frac{G_2}{h_2^p} (1+e^p)^2 \iint_p \left[ (\boldsymbol{\Psi}_u)^{\mathrm{T}} (\boldsymbol{\Psi}_u) + \frac{1-\nu_2^p}{2} (\boldsymbol{\Psi}_u)^{\mathrm{T}} (\boldsymbol{\Psi}_u) \right] \mathrm{d}x\, \mathrm{d}y$$

$$+ \frac{E_3 h_3}{1-(\nu_3)^2} \int_0^{l_y} \int_0^{l_x} \left[ \left(\frac{\partial}{\partial x}\boldsymbol{\Psi}_u\right)^{\mathrm{T}} \left(\frac{\partial}{\partial x}\boldsymbol{\Psi}_u\right) + \frac{1-\nu_3}{2} \left(\frac{\partial}{\partial y}\boldsymbol{\Psi}_u\right)^{\mathrm{T}} \left(\frac{\partial}{\partial y}\boldsymbol{\Psi}_u\right) \right] \mathrm{d}x\, \mathrm{d}y, \quad (21a)$$

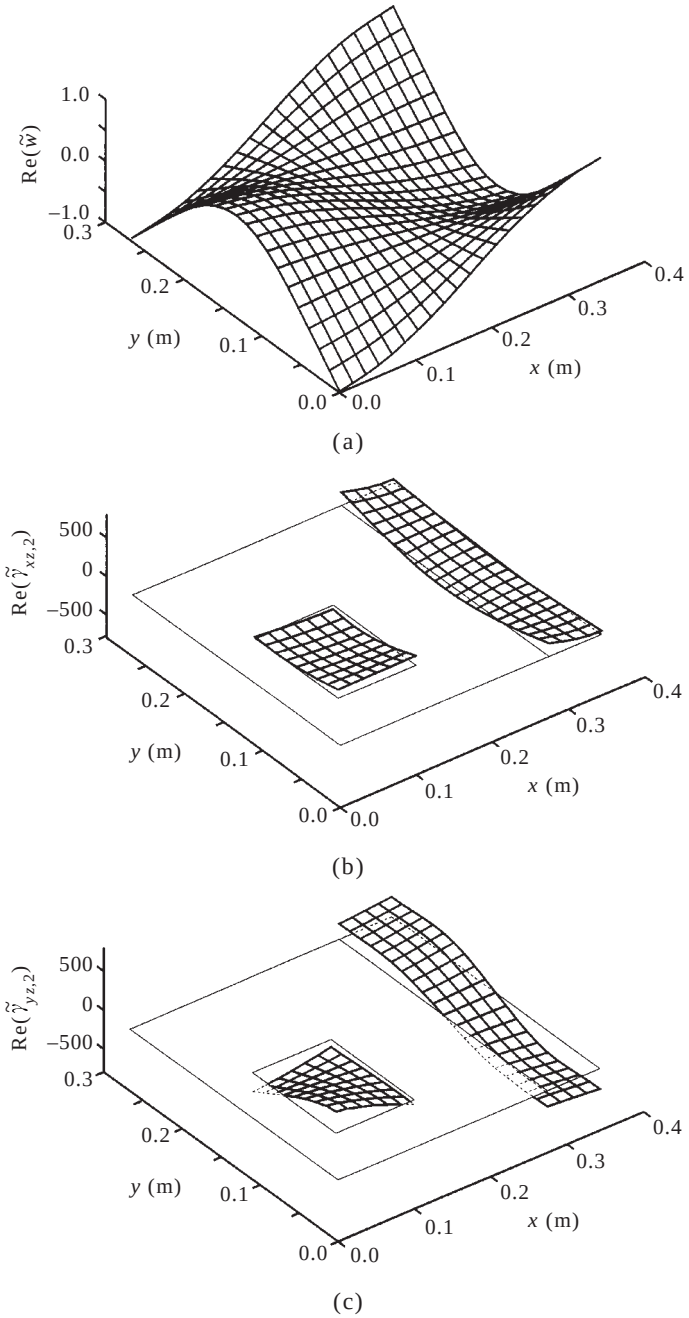


Figure 6. Real part of deformation mode shapes of Case C for mode (1, 2). (a) Flexural mode; (b) shear mode of layer 2 in the *xz* plane; (c) shear mode of layer 2 in the *yz* plane.

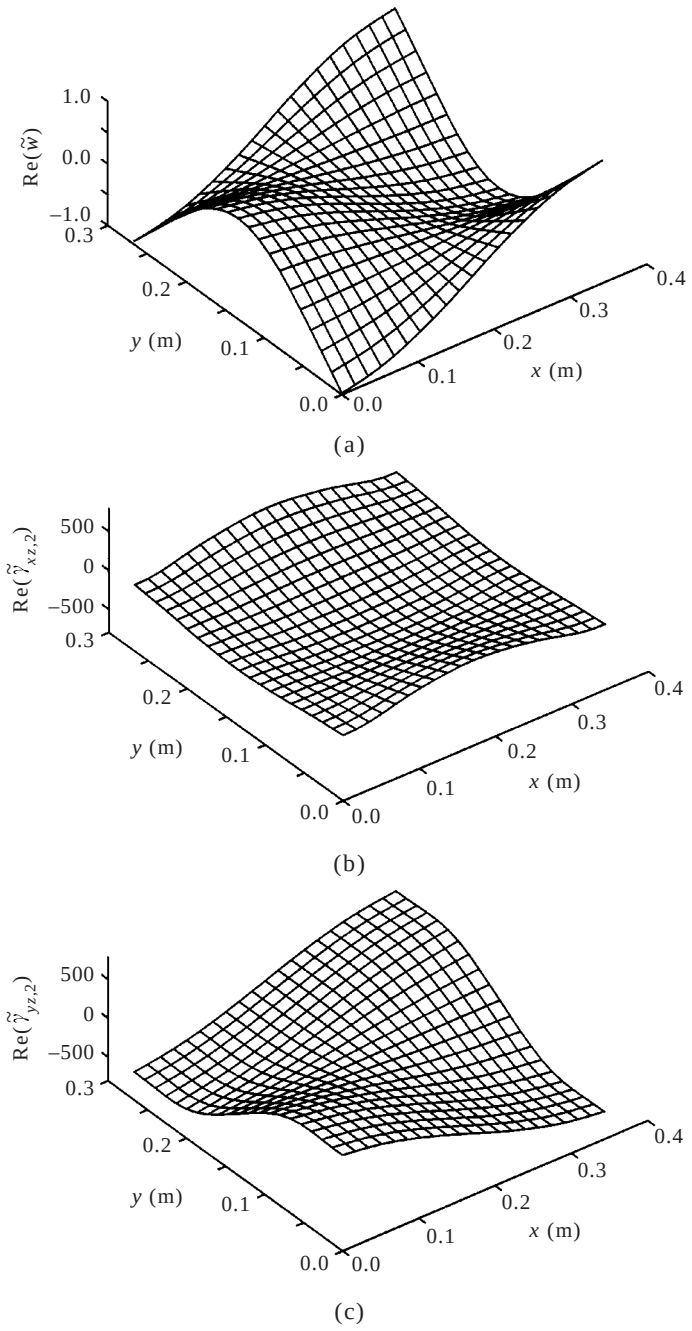


Figure 7. Real part of deformation mode shapes of the full coverage case (Case E) for mode (1, 2). (a) Flexural mode; (b) shear mode of layer 2 in the *xz* plane; (c) shear mode of layer 2 in the *yz* plane.

$$\mathbf{A}^{vv} = \sum_{p=1}^{N_p} \frac{E_3 h_3 e^p}{1-(v_3)^2} \iint_p \left[ \left( \frac{\partial}{\partial x} \boldsymbol{\Psi}_v \right)^{\mathrm{T}} \left( \frac{\partial}{\partial x} \boldsymbol{\Psi}_v \right) + \frac{1-v_1^p}{2} \left( \frac{\partial}{\partial y} \boldsymbol{\Psi}_v \right)^{\mathrm{T}} \left( \frac{\partial}{\partial y} \boldsymbol{\Psi}_v \right) \right] \mathrm{d}x \, \mathrm{d}y$$

$$+ \sum_{p=1}^{N_p} \frac{G_2}{h_2^p} (1+e^p)^2 \iint_p \left[ (\boldsymbol{\Psi}_v)^{\mathrm{T}} (\boldsymbol{\Psi}_v) + \frac{1-v_2^p}{2} (\boldsymbol{\Psi}_v)^{\mathrm{T}} (\boldsymbol{\Psi}_v) \right] \mathrm{d}x \, \mathrm{d}y$$

$$+ \frac{E_3 h_3}{1-(v_3)^2} \int_0^{l_y} \int_0^{l_x} \left[ \left( \frac{\partial}{\partial x} \boldsymbol{\Psi}_v \right)^{\mathrm{T}} \left( \frac{\partial}{\partial x} \boldsymbol{\Psi}_v \right) + \frac{1-v_3}{2} \left( \frac{\partial}{\partial y} \boldsymbol{\Psi}_v \right)^{\mathrm{T}} \left( \frac{\partial}{\partial y} \boldsymbol{\Psi}_v \right) \right] \mathrm{d}x \, \mathrm{d}y, \qquad (21b)$$

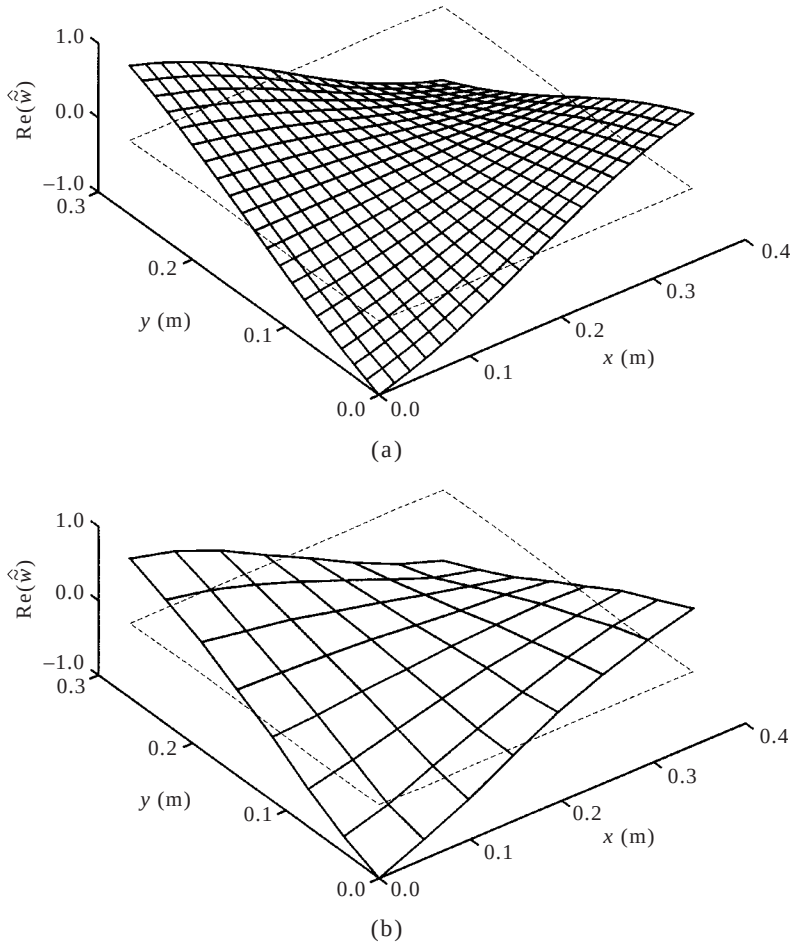


Figure 8. Real part of flexural mode shapes of mode (1, 1) for all five cases. (a) Prediction; (b) measurement.

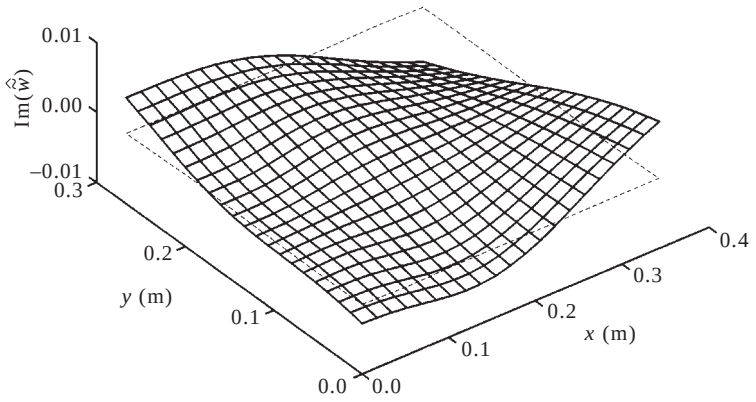


(a)

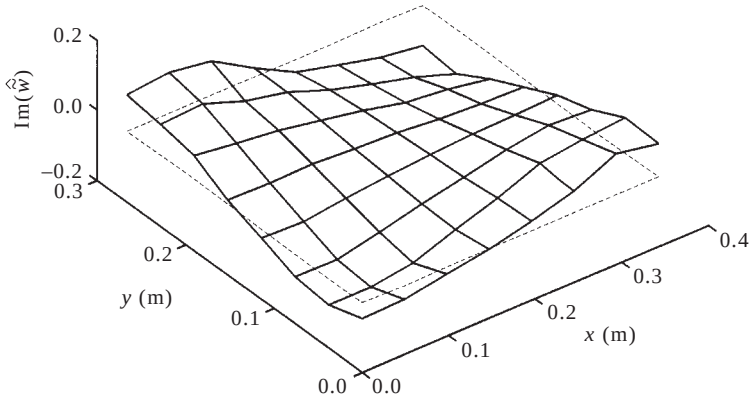


(b)

Figure 9. Imaginary part of flexural mode shapes of mode (1, 1) for Case A. (a) Prediction; (b) measurement.

$$\mathbf{A}^{uw} = \sum_{p=1}^{N_p} \frac{E_3 h_3 e^p}{1-(\nu_3)^2} \iint_p \left[ \nu_1 \left(\frac{\partial}{\partial x}\boldsymbol{\Psi}_u\right)^{\mathrm{T}} \left(\frac{\partial}{\partial y}\boldsymbol{\Psi}_v\right) + \frac{1-\nu_1^p}{2} \left(\frac{\partial}{\partial y}\boldsymbol{\Psi}_u\right)^{\mathrm{T}} \left(\frac{\partial}{\partial x}\boldsymbol{\Psi}_v\right) \right] \mathrm{d}x\, \mathrm{d}y$$

$$+ \frac{E_3 h_3}{1-(\nu_3)^2} \int_0^{l_y} \int_0^{l_x} \left[ \nu_3 \left(\frac{\partial}{\partial x}\boldsymbol{\Psi}_u\right)^{\mathrm{T}} \left(\frac{\partial}{\partial y}\boldsymbol{\Psi}_v\right) + \frac{1-\nu_3}{2} \left(\frac{\partial}{\partial y}\boldsymbol{\Psi}_u\right)^{\mathrm{T}} \left(\frac{\partial}{\partial x}\boldsymbol{\Psi}_v\right) \right] \mathrm{d}x\, \mathrm{d}y, \tag{21c}$$

$$\mathbf{A}^{vu} = \sum_{p=1}^{N_p} \frac{E_3 h_3 e^p}{1-(\nu_3)^2} \iint_p \left[ \nu_1 \left(\frac{\partial}{\partial y}\boldsymbol{\Psi}_u\right)^{\mathrm{T}} \left(\frac{\partial}{\partial x}\boldsymbol{\Psi}_v\right) + \frac{1-\nu_1^p}{2} \left(\frac{\partial}{\partial x}\boldsymbol{\Psi}_u\right)^{\mathrm{T}} \left(\frac{\partial}{\partial y}\boldsymbol{\Psi}_v\right) \right] \mathrm{d}x\, \mathrm{d}y$$

$$+ \frac{E_3 h_3}{1-(\nu_3)^2} \int_0^{l_y} \int_0^{l_x} \left[ \nu_3 \left(\frac{\partial}{\partial y}\boldsymbol{\Psi}_u\right)^{\mathrm{T}} \left(\frac{\partial}{\partial x}\boldsymbol{\Psi}_v\right) + \frac{1-\nu_3}{2} \left(\frac{\partial}{\partial x}\boldsymbol{\Psi}_u\right)^{\mathrm{T}} \left(\frac{\partial}{\partial y}\boldsymbol{\Psi}_v\right) \right] \mathrm{d}x\, \mathrm{d}y, \tag{21d}$$

$$\mathbf{A}^u = [(A^u)_1 \quad \cdots \quad (A^u)_p \quad \cdots \quad (A^u)_{N_p}]; \qquad (\mathbf{A}^u)_p = -\frac{(e^p+1)G_2^p}{h_2^p}\iint_p \mathbf{\Psi}_u \,\mathrm{d}x\,\mathrm{d}y, \quad (21e)$$

$$\mathbf{A}^v = [(A^v)_1 \quad \cdots \quad (A^v)_p \quad \cdots \quad (A^v)_{N_p}]; \qquad (\mathbf{A}^v)_p = -\frac{(e^p+1)G_2^p}{h_2^p}\iint_p \mathbf{\Psi}_u \,\mathrm{d}x\,\mathrm{d}y, \quad (21f)$$

$$\mathbf{A}^{\mathrm{d}x} = \begin{bmatrix} (A^{\mathrm{d}x})_1 & & & \mathbf{0} \\ & \ddots & & \\ & & (A^{\mathrm{d}x})_p & \\ & & & \ddots \\ \mathbf{0} & & & (A^{\mathrm{d}x})_{N_p} \end{bmatrix}, \qquad (\mathbf{A}^{\mathrm{d}x})_p = \frac{G_2^p I_x^p}{h_2^p}, \quad (21g)$$

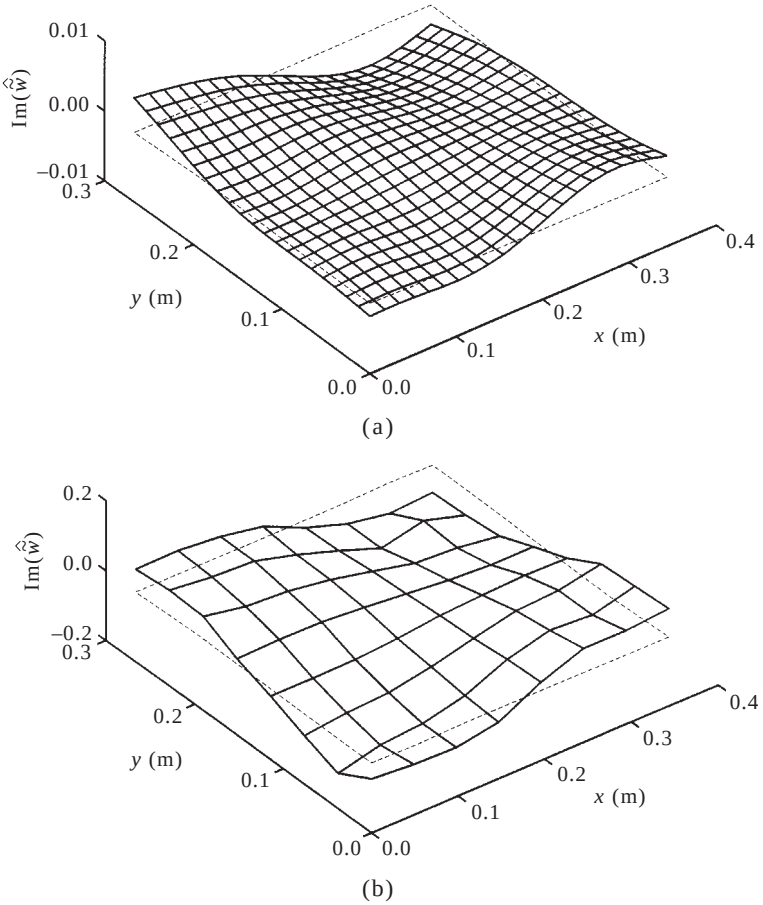


Figure 10. Imaginary part of flexural mode shapes of mode (1, 1) for Case B. (a) Prediction; (b) measurement.

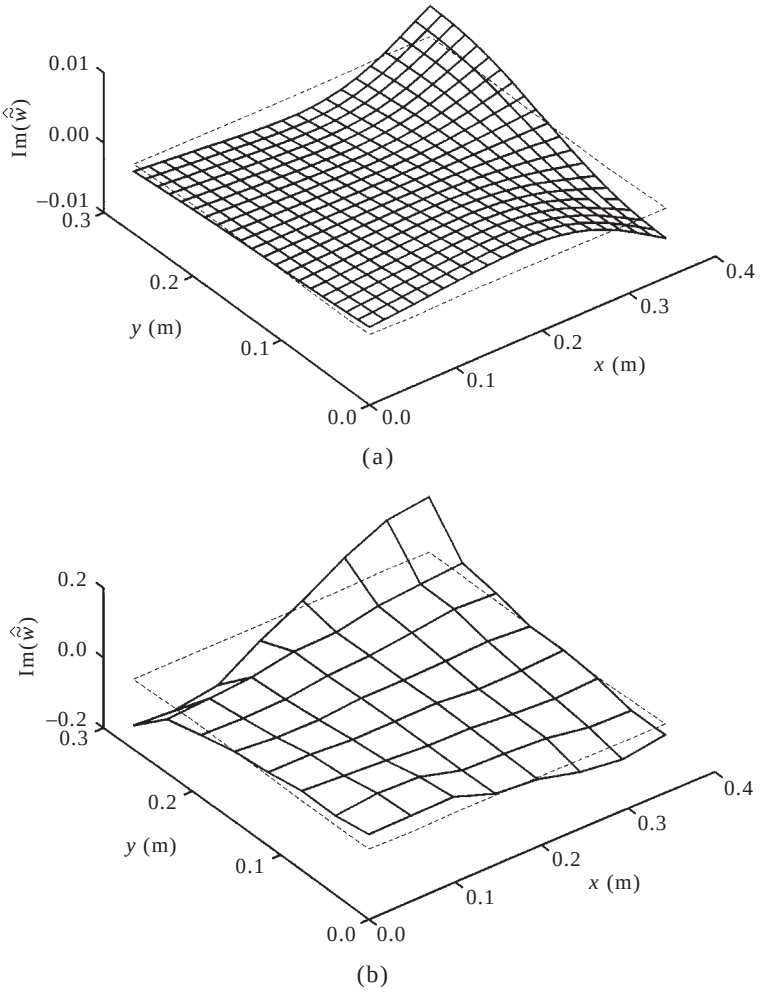


Figure 11. Imaginary part of flexural mode shapes of mode (1, 1) for Case C. (a) Prediction; (b) measurement.

$$\mathbf{A}^{\mathrm{dy}} = \begin{bmatrix} (A^{\mathrm{dy}})_1 & & \mathbf{0} \\ & \ddots & \\ & (A^{\mathrm{dy}})_p & \\ & & \ddots \\ \mathbf{0} & & (A^{\mathrm{dy}})_{N_p} \end{bmatrix}, \qquad (\mathbf{A}^{\mathrm{dy}})_p = \frac{G_2^p I_y^p}{h_2^p}, \tag{21h}$$

$$\mathbf{B}_k^u = \sum_{p=1}^{N_p} \frac{H^p(e^p+1)G_2^p}{h_2^p} \iint_p \left(\frac{\partial \phi_{w,k}}{\partial x}\right) \boldsymbol{\Psi}_u^{\mathrm{T}} \, \mathrm{d}x \, \mathrm{d}y, \tag{21i}$$

$$\mathbf{B}_k^v = \sum_{p=1}^{N} \frac{H^p(e^p+1)G_2^p}{h_2^p} \iint_p \left(\frac{\partial \phi_{w,k}}{\partial y}\right) \mathbf{\Psi}_v^{\mathrm{T}} \, \mathrm{d}x \, \mathrm{d}y, \tag{21j}$$

$$\mathbf{B}_k^{\mathrm{d}x} = [(\mathbf{B}_k^{\mathrm{d}x})_1 \quad \cdots \quad (\mathbf{B}_k^{\mathrm{d}x})_p \quad \cdots \quad (\mathbf{B}_k^{\mathrm{d}x})_{N_p}]^{\mathrm{T}},$$

$$(\mathbf{B}_k^{\mathrm{d}x})_p = -\frac{H^p(e^p+1)G_2^p}{h_2^p} \iint_p \left(\frac{\partial \phi_{w,k}}{\partial x}\right) \mathrm{d}x \, \mathrm{d}y, \tag{21k}$$

$$\mathbf{B}_k^{\mathrm{d}y} = [(\mathbf{B}_k^{\mathrm{d}y})_1 \quad \cdots \quad (\mathbf{B}_k^{\mathrm{d}y})_p \quad \cdots \quad (\mathbf{B}_k^{\mathrm{d}y})_{N_p}]^{\mathrm{T}},$$

$$(\mathbf{B}_k^{\mathrm{d}y})_p = -\frac{H^p(e^p+1)G_2^p}{h_2^p} \iint_p \left(\frac{\partial \phi_{w,k}}{\partial y}\right) \mathrm{d}x \, \mathrm{d}y, \tag{21l}$$

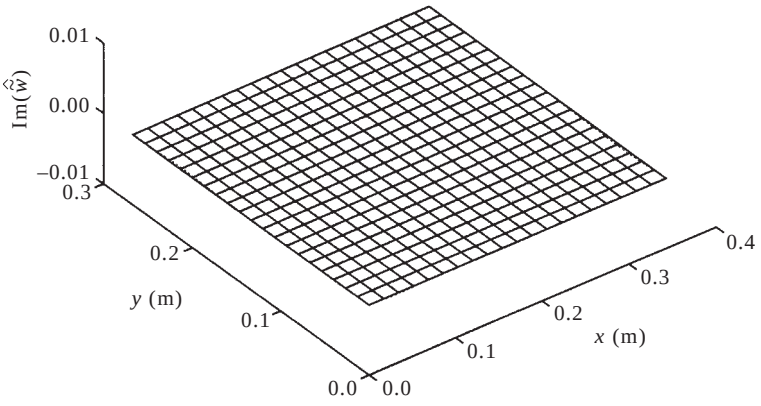


(a)

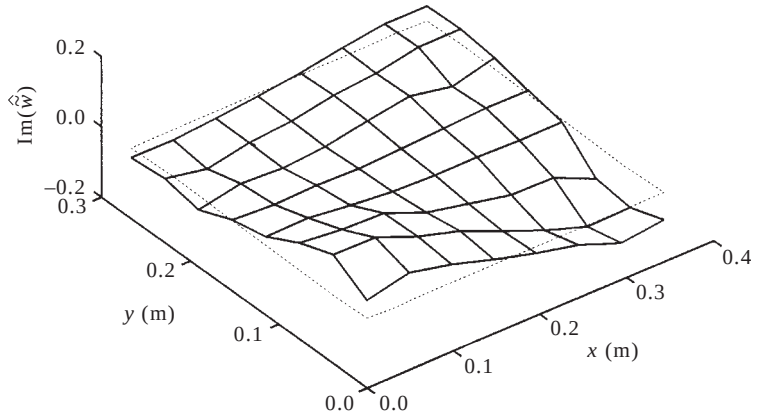


(b)

Figure 12. Imaginary part of flexural mode shapes of mode (1, 1) for Case D. (a) Prediction; (b) measurement.

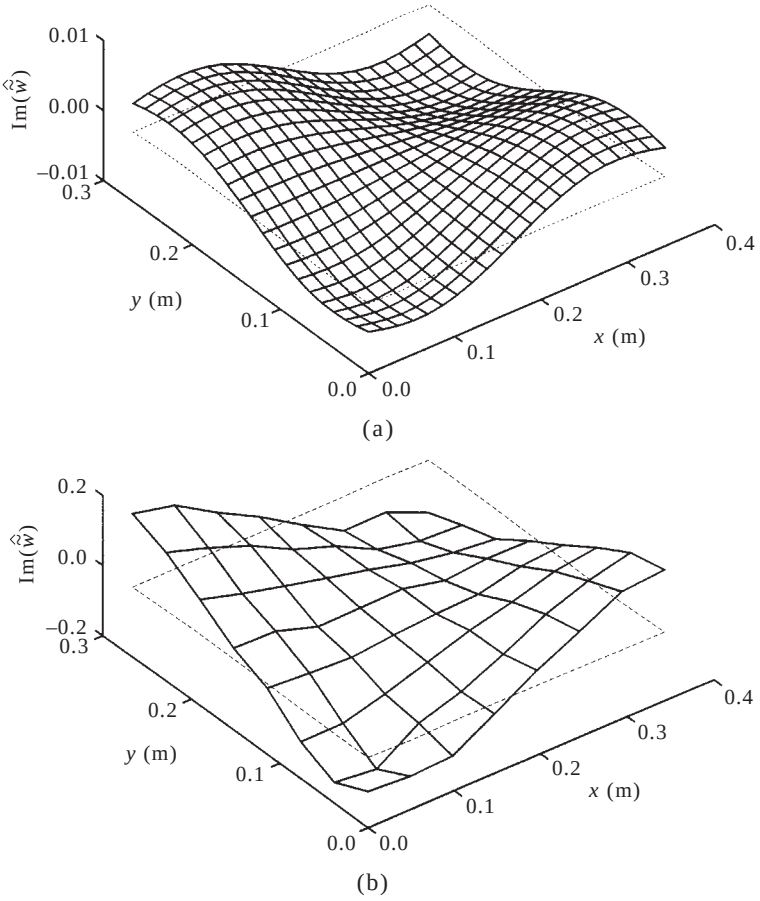


Figure 13. Imaginary part of flexural mode shapes of mode (1, 1) for Case E. (a) Prediction; (b) measurement.

TABLE 7

*Weighting factors $\alpha_r$ and $\beta_r$ for equation* (38) *as derived from analytical models*

| Mode $r$ | $\alpha_r$ | $\beta_r$ |
|---|---|---|
| 1 | 1·14 | 1·11 |
| 2 | 0·98 | 1·08 |
| 3 | 1·14 | 1·00 |
| 4 | 0·87 | 1·02 |
| 5 | 0·81 | 1·09 |
| 6 | 1·00 | 0·95 |
| 7 | 1·14 | 1·07 |
| 8 | 0·94 | 1·00 |

TABLE 8

*Comparison between calculated and estimated modal loss factors of Case C based on the analytical method*

| | $\eta_{r,C}$ (%) | | | | |
|---|---|---|---|---|---|
| | | Weighted additive method | | Simple additive method | |
| Mode $r$ | Calculated | Estimated | Error | Estimated | Error |
| 1 | 0·52 | 0·52 | 0 | 0·46 | 11 |
| 2 | 0·19 | 0·19 | 0 | 0·19 | −1 |
| 3 | 1·81 | 1·81 | 0 | 1·72 | 5 |
| 4 | 0·93 | 0·93 | 0 | 0·98 | −5 |
| 5 | 1·81 | 1·81 | 0 | 1·77 | 2 |
| 6 | 1·13 | 1·13 | 0 | 1·13 | 0 |
| 7 | 1·07 | 1·07 | 0 | 0·98 | 9 |
| 8 | 1·41 | 1·41 | 0 | 1·44 | −2 |

where $H^p = (h_1^p + 2h_2^p + h_3)/2$. The coefficients of $\mathbf{C}_k$ can be calculated by

$$\mathbf{C}_k = \mathbf{A}^{-1}\mathbf{B}_k \tag{22}$$

provided $|\mathbf{A}| \neq 0$. As a result, all entries in the $k$th shape function set $\mathbf{S}_{1,k}^p$, $\mathbf{S}_{2,k}^p$ and $\mathbf{S}_{3,k}$ can be determined for a given flexural shape function $\phi_{w,k}$. This process needs to be repeated $N_s$ times and then $\mathbf{C}$ is obtained as

$$\mathbf{C} = \begin{bmatrix} \mathbf{c}_u \\ \mathbf{c}_v \\ \mathbf{d}_x \\ \mathbf{d}_y \end{bmatrix} = \begin{bmatrix} \mathbf{c}_{u,1} & \cdots & \mathbf{c}_{u,k} & \cdots & \mathbf{c}_{u,N_s} \\ \mathbf{c}_{v,1} & \cdots & \mathbf{c}_{v,k} & \cdots & \mathbf{c}_{v,N_s} \\ \mathbf{d}_{x,1} & \cdots & \mathbf{d}_{x,k} & \cdots & \mathbf{d}_{x,N_s} \\ \mathbf{d}_{y,1} & \cdots & \mathbf{d}_{y,k} & \cdots & \mathbf{d}_{y,N_s} \end{bmatrix}. \tag{23}$$

Then the entire shape function matrices $\mathbf{S}_1^p$, $\mathbf{S}_2^p$ and $\mathbf{S}_3$ are determined.

TABLE 9

*Comparison between measured, calculated and estimated modal loss factors of Case C based on the experimental study. Estimation of $\eta_{r,C}$ without considering inherent damping of base plate*

| | $\eta_{r,C}$ (%) | | | |
|---|---|---|---|---|
| | | | Estimated | |
| Mode $r$ | Measured | Calculated[a] | Weighted | Simple |
| 1 | 0·52 | 0·52 | 0·72 | 0·64 |
| 2 | 0·52 | 0·19 | 0·63 | 0·62 |
| 3 | 1·97 | 1·81 | 1·91 | 1·84 |
| 4 | 0·88 | 0·93 | 0·96 | 1·01 |
| 5 | 1·93 | 1·81 | 1·93 | 1·86 |
| 6 | 2·30 | 1·13 | 2·17 | 2·18 |
| 7 | 1·00 | 1·07 | 1·07 | 0·97 |
| 8 | 1·97 | 1·41 | 1·58 | 1·60 |

[a] From Table 8.

TABLE 10

*Comparison between measured, calculated and estimated modal loss factors of Case C based on the experimental study. Estimation of $\eta_{r,\mathrm{CI}}$ with inherent damping measured in base plate*

| Mode $r$ | $\eta_{r,\mathrm{CI}}$ (%) | | | |
|---|---|---|---|---|
| | | | Estimated | |
| | Measured | Calculated[a] | Weighted | Simple |
| 1 | 0·52 | 0·84 | 0·31 | 0·31 |
| 2 | 0·52 | 0·34 | 0·47 | 0·47 |
| 3 | 1·97 | 1·88 | 1·83 | 1·77 |
| 4 | 0·88 | 1·06 | 0·85 | 0·88 |
| 5 | 1·93 | 1·88 | 1·87 | 1·79 |
| 6 | 2·30 | 1·20 | 2·10 | 2·11 |
| 7 | 1·00 | 1·13 | 1·00 | 0·91 |
| 8 | 1·97 | 1·45 | 1·54 | 1·56 |

[a] Table 8 value plus inherent damping found in experiments.

## 4. COMPLEX EIGENVALUE FORMULATION

For harmonic vibration analysis at frequency $\omega$, the complex-valued Young's modulus and shear modulus of the viscoelastic material in layer 2 of patch $p$ are represented by

$$\tilde{E}_2^p(\omega) = E_2^p(1 + \mathrm{i}\eta_2^p(\omega)), \qquad \tilde{G}_2^p(\omega) = G_2^p(1 + \mathrm{i}\eta_2^p(\omega)), \tag{24a, b}$$

where $\mathrm{i} = \sqrt{-1}$, and $\eta_2^p$ is the material loss factor. Using equations (2), (6) and (8), rewrite strain and kinetic energies in the complex-valued form as

$$\tilde{U} = \tfrac{1}{2}\mathbf{q}^{\mathrm{T}}\tilde{\mathbf{K}}\mathbf{q}, \qquad T = \tfrac{1}{2}\dot{\mathbf{q}}^{\mathrm{T}}\mathbf{M}\dot{\mathbf{q}}, \tag{25a, b}$$

where the complex-valued stiffness ($\tilde{\mathbf{K}}$) and real-valued mass ($\mathbf{M}$) matrices of the system are defined as follows from equations (2) and (6)

$$\tilde{\mathbf{K}} = \sum_{p=1}^{N_p} \iint_p [(\mathscr{D}\mathbf{S}_1^p)^{\mathrm{T}}\mathbf{E}_1(\mathscr{D}\mathbf{S}_1^p) + (\mathscr{D}\mathbf{S}_2^p)^{\mathrm{T}}\tilde{\mathbf{E}}_2(\mathscr{D}\mathbf{S}_2^p)]\,\mathrm{d}x\,\mathrm{d}y + \int_0^{l_y}\int_0^{l_x} (\mathscr{D}\mathbf{S}_3)^{\mathrm{T}}\mathbf{E}_3(\mathscr{D}\mathbf{S}_3)\,\mathrm{d}x\,\mathrm{d}y,$$

$$\mathbf{M} = \sum_{p=1}^{N_p} \int_p [\mathbf{S}_1^{p\,\mathrm{T}}\mathbf{H}_1\mathbf{S}_1^p + \mathbf{S}_2^{p\,\mathrm{T}}\mathbf{H}_2\mathbf{S}_2^p]\,\mathrm{d}x + \int_0^l \mathbf{S}_3{}^{\mathrm{T}}\mathbf{H}_3\mathbf{S}_3\,\mathrm{d}x. \tag{26a, b}$$

The complex eigenvalue problem of dimension $N_s$ is then formulated for the following matrix form of governing equations:

$$\mathbf{M}\ddot{\mathbf{q}} + \tilde{\mathbf{K}}\mathbf{q} = \mathbf{0}. \tag{27}$$

Eigenvalues ($\tilde{\lambda}_r$) and eigenvectors ($\tilde{g}_r$) of this non-proportionally damped system problem are complex-valued where $r$ is the modal index. The undamped natural frequencies ($\omega_r$) and composite modal loss factors ($\eta_r$) are related to $\tilde{\lambda}_r$ of equation (27) in the following manner [1]:

$$\omega_r = \sqrt{\mathrm{Re}\,(\tilde{\lambda}_r)}, \qquad \eta_r = \frac{\mathrm{Im}\,(\tilde{\lambda}_r)}{\mathrm{Re}\,(\tilde{\lambda}_r)}; \qquad r = 1, \ldots, N_s. \tag{28a, b}$$

Complex mode shapes of relevant deformation variables can be calculated from the resulting eigenvectors $\tilde{q}_r$ of equation (27). For example, the complex flexural mode shape is

$$\tilde{w}_r(x, y) = \Phi_w(x, y)\tilde{q}_r. \tag{29}$$

Complex in-plane mode shapes of layer 3 in $x$ and $y$ directions are

$$\tilde{u}_{3,r}(x, y) = \mathbf{\Psi}_u(x, y)\mathbf{c}_u\tilde{q}_r, \qquad \tilde{v}_{3,r}(x, y) = \mathbf{\Psi}_v(x, y)\mathbf{c}_v\tilde{q}_r. \tag{30a, b}$$

Complex shear deformation mode shapes of layer 2 in $xz$ and $yz$ planes are

$$\tilde{\gamma}^p_{xz2,r}(x, y) = \frac{1}{h_2^p}\left[H^p\frac{\partial\mathbf{\Phi}_w(x, y)}{\partial x} - (1 + e^p)\mathbf{\Psi}_u(x, y)\mathbf{c}_u + \mathbf{d}^p_x\right]\tilde{q}_r,$$

$$\tilde{\gamma}^p_{yz2,r}(x, y) = \frac{1}{h_2^p}\left[H^p\frac{\partial\mathbf{\Phi}_w(x, y)}{\partial y} - (1 + e^p)\mathbf{\Psi}_v(x, y)\mathbf{c}_v + \mathbf{d}^p_y\right]\tilde{q}_r. \tag{31a, b}$$

## 5. COMPARISON WITH LITERATURE

To validate the proposed theory, consider a rectangular plate (of dimension $l_x$ and $l_y$) with simple supports along all edges. This case with full surface damping has been analyzed by Lall *et al*. [4], Mead (as reported in reference [4]) and He and Ma [5]. In particular, He and Ma [5] have provided a closed form equation for full coverage. System parameters, as defined by Lall *et al*. [4], are summarized in Table 1. For our study, analytical solutions are obtained by using four flexural shapes of sine functions in each $\mathbf{X}_w$ or $\mathbf{Y}_w$. Also the in-plane trial functions in $u$ and $v$ are constructed by using four trial functions for each direction $x$ or $y$, resulting in matrix $\mathbf{A}$ of equation (18) of size 32. For each flexural shape function $\phi_{w,k}(x, y)$, vector $\mathbf{B}_k$ is constructed and coefficients in vector $\mathbf{C}_k = \mathbf{A}^{-1}\mathbf{B}_k$ are calculated to determine the $k$th shape function set $\mathbf{S}^p_{1,k}$, $\mathbf{S}^p_{2,k}$ and $\mathbf{S}_{3,k}$. Then the entire shape function matrices $\mathbf{S}^p_1$, $\mathbf{S}^p_2$ and $\mathbf{S}_3$ set are incorporated in the Rayleigh–Ritz minimization scheme to obtain the complex-valued eigenvalue problem of size 16. Natural frequencies and modal loss factors are then obtained by using equation (28) after solving the eigenvalue problem.

First consider a simply supported square plate with full coverage, labelled here as Example 1 in Table 1. Natural frequencies and modal loss factors of the first four modes obtained from the literature [4, 5] are compared with results of our method. It is seen in Table 2 that our predictions are nearly identical to the results of Mead [4] and He and Ma [5]. They also match the results reported by Lall *et al*. [4] even though minor discrepancies are seen. All methods essentially predict same results.

For Example II of Table 1, the base plate is kept the same but a square damping patch of varying size ($l^p_x = l^p_x = l^p$) as shown in Figure 3 is applied. This case was specifically studied by Lall *et al*. [4]. Both layers (1 and 2) of the patch are thinner and the viscoelastic core is stiffer than described in Example 1. Parametric studies of patch size ($l^p$) variation for the first natural frequency and modal loss factor as reported by Lall *et al*. [4] are carried out and results are in Figure 4. Poor agreement between the two methods is seen. Next, He and Ma's closed form solution [5] is used again for the full treatment case. It is seen that our results indeed match the closed form solution for the limiting case of $l^p = l$. Further validation is necessary and it is established through a series of modal experiments as presented in the next section.

## 6. EXPERIMENTAL VERIFICATION

### 6.1. EXAMPLE CASES

A rectangular plate ($l_x = 342{\cdot}9$ mm, $l_y = 266{\cdot}7$ mm) under the F–F–F–F boundary conditions is chosen as the benchmark example to experimentally verify our analytical model where F denotes a free boundary. The plate is suspended freely and excited with an impulse hammer. Structural acceleration is measured via a compact accelerometer (of weight 1 g) that is attached near one corner of the plate. Response signals are fed to the analyzer along with the excitation force and sinusoidal transfer functions are obtained. First eight natural frequencies ($f_r$) and modal loss factors ($\eta_r$) are then extracted using the half-power bandwidth method [1]. Two types of damping patches (designated here as Patches A and B) with material properties and layer thickness, as specified in Table 3, are applied in this study. Material properties of the viscoelastic core are obtained by adopting the material property estimation technique we had developed earlier in reference [1]. Frequency-dependent material loss factor $\eta_2(\omega)$ and shear modulus $G_2(\omega)$ are obtained for each damping patch. Since the variation in $G_2$ is very small in the frequency range of interest, $G_2$ may be safely assumed to be spectrally-invariant in order to avoid solving the eigenvalue problem with a frequency-dependent stiffness matrix.

Five damping cases for the rectangular plate including limiting cases are considered here, as illustrated schematically in Figure 5. Case A denotes the plate with a single patch (Patch A) attached away from all edges. Case B is the plate with Patch B attached at the edge. The plate with both Patches A and B applied simultaneously is designated as Case C. Two limiting cases constitute the baseline studies: Case D is the undamped base plate without any damping patch, and Case E is the full coverage case when the plate is fully covered on one side with Patch A material only. Many other damping configurations are possible but these five cases are believed to be necessary and hence only these results are presented here.

### 6.2. MODAL RESULTS

Natural frequencies and modal loss factor for the first eight modes have been measured. Corresponding predictions are then obtained by using the analytical procedure as discussed earlier. The number of shape functions is increased from four to eight and free–free beam mode shapes are used as flexural trial shapes in both $x$ and $y$ directions. The material loss factor of the viscoelastic core is assumed to be constant at the vicinity of a mode and only one eigenvalue problem is solved for each mode. In addition, mode shapes are obtained from eigenvectors $\tilde{q}_r$ by using equations (29)–(31). Modal indices that described nodal lines along $x$ and $y$ directions are listed in Table 4. Comparisons of modal results as listed in Table 5 and 6 show excellent agreement between experiment and theory for all cases.

One advantage of our method is the ease with which mode shapes of all deformation variables may be viewed. Of importance here are the shear deformation modes of the viscoelastic core in the $xz$ and $yz$ planes since they are the major contributors to the total energy dissipation; note that these modes can not be measured. Figure 6 shows the predicted flexural and shear deformation shapes of mode (1, 2) for Case C; compare these with the results of Figure 7 for the full coverage case (E). It is observed that shear modes of layer 2 in Case C show only segments of the full shapes corresponding to Case E. Also, the amplitude of shear modes in the $xz$ plane ($\gamma_{xz,2}$) is lower than that in the $yz$ plane ($\gamma_{yz,2}$). This can be explained simply by examining curvatures of the flexural mode in the $x$ and $y$ directions. Since the flexural mode is close to a straight line along the $y$ direction, the viscoelastic core experiences small shear deformations in the $xz$ plane ($\gamma_{xz,2}$). Conversely, the large curvature in the $y$ direction causes large shear deformations in the $yz$ plane ($\gamma_{yz,2}$).

### 6.3. COMPLEX MODE SHAPES

Since the system is non-porportionally damped, complex modes need to be normalized [6] before making any comparison between theory and experiment. The normalization has to be carried out in the spatial domain on flexural mode shapes $\tilde{w}_r(x, y)$ instead of considering a column of eigenvectors ($\tilde{\varphi}_r$). The normalized expression of the flexural mode $\hat{\tilde{w}}_r$ in terms of phase angle and amplitude are

$$\hat{\tilde{w}}_r(x, y) = \frac{\tilde{w}_r(x, y)\, e^{i\theta_{min}}}{|\tilde{w}_r(x_{max}, y_{max})|}, \tag{32}$$

where $\hat{}$ denotes normalized values, $|\ |$ is the operator for absolute value, $\theta_{min}$ is the rotating angle used for normalization, and $(x_{max}, y_{max})$ indicates the location of the largest flexural amplitude. The normalization of amplitude is straight forward but the rotating angle $\theta_{min}$ needs to be calculated such that the norm of the imaginary part of the normalized flexural mode Im $(\hat{\tilde{w}}\, e^{i\theta})$ is minimum.

Define a function $F(\theta)$ that is the spatial mean-square value of Im$(\tilde{w}\ e^{i\theta})$ when integrated over the plate surface, where $\theta$ is an arbitrary angle of rotation:

$$F(\theta) = \iint (\text{Im}\ (\tilde{w}\ e^{i\theta}))^2\, dx\, dy = \iint (\text{Re}\ (\tilde{w}) \sin\theta + \text{Im}\ (\tilde{w}) \cos\theta)^2\, dx\, dy. \tag{33}$$

Define $\theta_{min}$ as the angle when $F(\theta)$ reaches its minimum value. A necessary condition derived from $\partial F(\theta)/\partial\theta = 0$ is

$$\theta_{min} = \tfrac{1}{2} \tan^{-1} \left[ \frac{-2 \iint \text{Re}\ (\tilde{w})\ \text{Im}\ (\tilde{w})\, dx\, dy}{\iint [\text{Re}\ (\tilde{w})^2 - \text{Im}\ (\tilde{w})^2]\, dx\, dy} \right]. \tag{34}$$

The angle has to be examined by the following expression to ensure that $F(\theta_{min})$ is indeed the minimum value instead of being maximum:

$$\frac{\partial^2 F(\theta_{min})}{\partial\theta^2} = 2 \iint [(\text{Re}\ (\tilde{w}) \cos\theta - \text{Im}\ (\tilde{w}) \sin\theta)^2 - (\text{Re}\ (\tilde{w}) \sin\theta + \text{Im}\ (\tilde{w}) \cos\theta)^2]\, dx\, dy > 0. \tag{35}$$

Otherwise, $\theta_{min}$ must be rotated by $\pi/2$. Note that when the plate surface mode shape is described in terms of discrete points, for example in the measured data-set, the integration operator of equations (33–35) is replaced by a double summation.

After normalization, the real part (Re) and the imaginary part (Im) of predicted mode shapes can be compared with those measured. Figure 8 shows the real part of the normalized mode shape for mode (1, 1). Note that the real parts of the first mode shapes are almost the same for all five cases. Figures 9–13 show the imaginary part of the measured and predicted mode shapes for all five cases. It seems that the imaginary parts vary slightly depending on the damping configuration. Comparison between predictions and measurements again shows excellent agreement for each case.

## 7. DESIGN STUDY: ADDITIVE EFFECT OF PATCHES

Cases A, B and C are further examined to see how the damping patches add modal damping to the plate. Since Case C is a combination of Cases A and B, modal loss factors

of Case C may be estimated by using the results of Cases A and B in a weighted additive manner; this procedure was introduced earlier in reference [1] with application to beams:

$$\eta_{r,\mathrm{C}} = \alpha_r \eta_{r,\mathrm{A}} + \beta_r \eta_{r,\mathrm{B}}, \tag{36}$$

where subscripts A, B and C are the case designations defined earlier and $\alpha_r$ and $\beta_r$ are the weighting factors for mode $r$. Note that $\alpha_r$ and $\beta_r$ can be obtained using the analytical method, and sample values are listed in Table 7. However, practically it is more convenient to use the simple additive estimation procedure where $\alpha_r = \beta_r = 1$. Table 8 shows the comparison of both weighted and simple additive estimations with calculated values of $\eta_{r,\mathrm{C}}$. Errors introduced by the simple additive estimation method are less than 10% for most of the modes.

Both estimation procedures are next applied to our benchmark experimental study but the weighting factors are again obtained from the analytical model. Table 9 compares both estimations with measurements. It is seen that both methods provide reasonable estimates except for the first two modes. It may be explained from the fact that the base plate used for the experimental studies (Case D in Figure 5 and Table 6) has high inherent damping, especially at $r = 1, 2$. Therefore, the two estimation methods are modified and the inherent damping must be taken into account in an additive manner. Measured modal loss factors are considered to have contributions from inherent (I) damping of the base plate and applied patch damping (A, B or C) based on a simple additive estimation method:

$$\eta_{r,\mathrm{AI}} = \eta_{r,\mathrm{I}} + \eta_{r,\mathrm{A}}, \qquad \eta_{r,\mathrm{BI}} = \eta_{r,\mathrm{I}} + \eta_{r,\mathrm{B}}, \qquad \eta_{r,\mathrm{CI}} = \eta_{r,\mathrm{I}} + \eta_{r,\mathrm{C}}, \tag{37a–c}$$

The values of inherent damping $\eta_{r,\mathrm{I}}$ are found from the modal measurements on the baseline case. A refined estimate for the modal damping of Case C is introduced based on the weighted additive method as

$$\begin{aligned} \eta_{r,\mathrm{CI}} &= \iota_r \eta_{r,\mathrm{I}} + \alpha_r \eta_{r,\mathrm{A}} + \beta_r \eta_{r,\mathrm{B}} \\ &= \iota_r \eta_{r,\mathrm{I}} + \alpha_r (\eta_{r,\mathrm{AI}} - \eta_{r,\mathrm{I}}) + \beta_r (\eta_{r,\mathrm{BI}} - \eta_{r,\mathrm{I}}), \end{aligned} \tag{38}$$

where $\iota_r$ is the weighting factor for inherent damping whose value is taken as unity here. Table 10 shows estimates with inherent damping considered by both weighted and simple additive methods. In comparison with measurements, it is seen that, unlike the methods without inherent damping, both methods underestimate modal loss factors especially for the first two modes. Note that in Table 10 the calculated values from the analytical method also include inherent damping found in measurements. Tables 9 and 10 show that the estimate of second mode is considerably improved when the inherent damping is considered. Minor changes in other modes are seen. Overall, it is concluded that the additive estimation is a reasonable design prediction scheme but suitable weighting factors should be needed for improvements.

## 8. CONCLUSION

A new analytical model of a rectangular plate with multiple constrained layer damping patches has been developed to predict complex eigensolutions. Comparison with the work of three prior investigators [4, 5] on a simply supported plate validates the model for limiting case of full coverage. Analytical predictions of natural frequencies, modal loss factors and complex modes for a rectangular plate with one or two patches are in excellent agreement with modal measurements. In addition, a normalization scheme for complex mode shapes has been developed for comparing a measured and predicted mode shapes. A parametric design study has also been performed for a plate with two damping patches.

Again, good agreement is seen between theory, experiment and simplified estimation methods.

The method proposed in this article illustrates the importance of the kinematic relationships between flexural deformation shapes and other deformation variables including shear deformations of the viscoelastic core which are the major contributors to the overall energy dissipation. The visualization of the flexural mode and its associated shear deformations modes may explain why a damping patch at a certain location results in higher damping performance for a certain mode than at other patch locations. Further work is needed to optimize the selective damping treatment concept [7]. Also, the availability of the complex mode shapes will assist in the calculation of the structural intensities [8].

## ACKNOWLEDGMENTS

This research has been supported by the Army Research Office (URI Grant DAAL 03-92-G-0120; 1992-97; Project Monitor: Dr T. L. Doligalski). We thank the Wolverine Gasket Company for providing the damping material.

## REFERENCES

1. S.-W. Kung and R. Singh 1998 *Journal of Sound and Vibration* **212**, 781–805. Vibration analysis of beams with multiple constrained layer damping patches.
2. A. D. Nashif, D. I. G. Jones and J. P. Henderson 1985 *Vibration Damping*. New York: John Wiley.
3. C. T. Sun and Y. P. Lu 1995 *Vibration Damping of Structural Elements*. Englewood Cliffs, NJ: Prentice Hall.
4. A. K. Lall, N. T. Asnani and B. C. Nakra 1987 *Journal of Vibration, Acoustics, Stress, and Reliability in Design* **109**, 241–247. Vibration and damping analysis of rectangular plate with partially covered constrained viscoelastic layer.
5. J.-F. He and B.-A. Ma 1988 *Journal of Sound and Vibration* **126**, 37–47. Analysis of flexural vibration of viscoelastically damped sandwich plates.
6. G. Prater, Jr. and R. Singh 1990 *Journal of Sound and Vibration* **143**, 125–142. Eigenproblem formulation, solution and interpretation for non-proportionally damped continuous beams.
7. S.-W. Kung and R. Singh *Journal of Sound and Vibration* (accepted for publication). Development of approximate methods for the analysis of patch damping design concepts.
8. A. B. Spalding and J. A. Mann III 1995 *Journal of the Acoustical Society of America* **97**, 3617–3624. Placing small constrained layer damping patches on a plate to attain global or local velocity changes.

## APPENDIX: LIST OF SYMBOLS

| | |
|---|---|
| A,B,C,D,E | damping cases of benchmark experiments |
| $\mathbf{A}$ | governing equation matrix |
| $\mathbf{a},\mathbf{b},\mathbf{c}$ | cofficient vectors |
| $a,b,c$ | coefficients |
| $\mathbf{B}$ | governing equation vector |
| $\mathbf{C}$ | coefficient vector |
| $\mathbf{d}$ | spatial matrix |
| $d$ | spatial constant |
| $\mathbf{E}$ | elasticity matrix |
| $E$ | Young's modulus |
| $e$ | elasticity ratio $E_3A_3/E_1A_1$ |
| $F$ | function used to normalize modes |
| $f$ | frequency (Hz) |
| $G$ | Shear modulus |

| | |
|---|---|
| $\mathbf{H}$ | inertia matrix |
| $H$ | thickness parameter $(h_1 + 2h_2 + h_3)/2$ |
| $h$ | thickness |
| i | $\sqrt{-1}$ |
| $\mathbf{K}$ | stiffness matrix |
| $l$ | length |
| $\mathbf{M}$ | mass matrix |
| $N_p$ | total number of patches |
| $N_s$, $N_x$, $N_y$ | total number of shape functions |
| $\mathbf{q}$ | generalized displacement vector |
| $q$ | generalized displacement |
| $\not{e}$ | eigenvector |
| $\mathbf{r}$ | deformation vector |
| $\mathbf{S}$ | admissible shape function matrix |
| $T$ | kinetic energy |
| $u$,$v$ | in-plane or longitudinal displacement |
| $U$ | potential or strain energy |
| $\mathbf{V}$ | transfer matrix |
| $w$ | flexural displacement |
| $\mathbf{X}$,$\mathbf{Y}$ | shape function vectors in $x$ and $y$ |
| $x$,$y$,$z$ | spatial coordinates |
| $\alpha.\beta,\iota$ | modal weighting factors |
| $\boldsymbol{\Phi}$ | shape function vector |
| $\phi$ | shape function |
| $\gamma$ | shear deformation |
| $\lambda$ | eigenvalue |
| $\omega$ | frequency (rad/s) |
| $\eta$ | loss factor |
| $\rho$ | mass density |
| $\boldsymbol{\Psi}$ | trial function vector |
| $\psi$ | rotation |
| $\theta$ | rotation angle used to normalize complex mode |

*Operators*

| | |
|---|---|
| Col | matrix operator |
| $\mathscr{D}$ | differential operator matrix |
| Im | imaginary part |
| Re | real part |
| $\partial$ | differential operator |
| $\|$ | absolute value |

*Superscripts*

| | |
|---|---|
| $p$ | patch number |
| T | transpose |
| $\tilde{}$ | complex valued |
| $\hat{}$ | normalized quantity |

*Subscripts*

| | |
|---|---|
| A,B | type of damping patch |
| C | damping Case C |
| I | inherent damping |
| $i$ | layer number |
| $k$,$m$,$n$ | admissible function number |
| $max$ | maximmum |
| $min$ | minimum |
| $r$ | modal index |
| $u$,$v$, | in plane motion |

| | |
|---|---|
| $x,y,z$ | spatial coordinates |
| $w$ | flexural motion |
| $\gamma$ | shear deformation |
| $\psi$ | rotation |
| 1 | layer 1 (elastic constraining layer) |
| 2 | layer 2 (viscoelastic constrained layer) |
| 3 | layer 3 (base structure) |